Thermal Cycling Behavior of Bi-layer $Yb_2Si_2O_7$/SiC EBC Coated C_f/SiC Composites in Burner Rig Tests

Sian Chen
National Defence University
Pengju Chen
Central South University
Junjie Duan
Central South University
Maolin Chen
Central South University
Peng Xiao
Central South University
Yang Li
Central South University
Y. Li (liyang16@csu.edu.cn)
Powder Metallurgy Research Institute, Central South University, Changsha 410083, China

Research Article

Keywords: YbDS/SiC, Sol-gel, Gas scour, Oxidation

Posted Date: January 13th, 2021

DOI: https://doi.org/10.21203/rs.3.rs-142226/v1

Abstract

To improve the oxidation resistance of carbon fiber reinforced SiC ceramic matrix composites (C_f/SiC) at high-temperature and high-speed gas scour environment in burner rig tests, a novel bi-layer $Yb_2Si_2O_7$/SiC EBC was prepared on the surface of C_f/SiC composites by chemical vapor deposition (CVD) and sol-gel method united with air spraying. Results show that bi-layer $Yb_2Si_2O_7$/SiC coating showed better oxidation resistance for C_f/SiC specimens before 20 thermal cycles (300 min), which can efficiently prevent the oxidation of C_f/SiC specimens in a gas scour environment at 1773 K for 300 min with a weight loss of 5.93×10^{-3} g·cm^{-2}. After 20 thermal cycles (≥300 min), the weight loss of the coated specimen is rapidly increased due to the formation of penetrating cracks. After the corrosion of 36 thermal cycles (540 min), some obvious annular corrosion pit area were found on the surface of $Yb_2Si_2O_7$ outer coating, the center of the corrosion pit was easier to be the origin area of the cracks due to the greater impact force of the gas.

Introduction

Silicon-based ceramics and composites such as carbon fiber reinforced SiC ceramic matrix composites (C_f/SiC) are prime candidates for high-temperature structural materials of the gas turbine, heat-exchanger parts, rocket nozzles, etc owing to their light weight and excellent thermal and mechanical [1-3]. However, the carbon fiber in C_f/SiC composites is quickly oxidized when exposed in an extreme high-temperature and oxygen enriched operating environment [4-7]. Therefore, it is essential to prepare environmental barrier coatings (EBCs) on the external of C_f/SiC composites to improve their adaptability to extreme operating environments.

During the past few decades, many researchers had studied bi-layer EBCs systems to improve the oxidation resistance of C_f/SiC composites [8-14], such as mullite/SiC [8], $ZrSiO_4$/SiC [9], BSAS/SiC [10], $Er_2Si_2O_7$/SiC [11] etc. Atmospheric plasma spraying (APS) and electron beam physical vapor deposition (EB-PVD) are two main methods to prepare EBCs on C_f/SiC composites at present [15, 16]. Besides, there are various methods to manufacture the EBCs on C_f/SiC composites, such as suspension plasma spraying (SPS), chemical vapor deposition (CVD), electrophoretic deposition, sol–gel methods, etc [17-19]. But, the above methods were either complicated in process or not suitable for the preparation of large and special-shaped parts.

Si or SiC ceramics are usually used as the bond layer in EBCs owing to their good chemical and physical compatibility with C_f/SiC composites, and the SiO_2 film formed by the oxidation can effectively prevent the diffusion of oxygen to the C_f/SiC matrix [16]. Rare earth ytterbium silicate ($Yb_2Si_2O_7$, YbDS) ceramic is a candidate coating due to the high melting point (2123 K), good chemical stability, and similar coefficient of thermal expansion (CTE) ($4–6 \times 10^{-6}$/K) to Si ($3.5–4.5 \times 10^{-6}$/K) or SiC ($4.3–5.4 \times 10^{-6}$/K) ceramic [20, 21]. The experimental and first-principles calculation results showed that the YbDS ceramic had the best corrosion resistance to water vapor environment in rare earth silicate ceramics (Yb, Sc, Y, Lu,

etc) [22, 23]. In our previous work, the oxidation behavior of bi-layer YbDS/SiC EBCs covered C_f/SiC composites in the air environment at 1773 K had been studied [24], which showed that YbDS/SiC coating can provide long-term oxidation resistance for C_f/SiC composite. However, few researchers have studied the oxidation behavior of bi-layer YbDS/SiC EBCs covered C_f/SiC composites in the burner rig tests at high-temperature (≥1773 K).

In this work, the bi-layer YbDS/SiC EBCs was prepared to study the stability of the coating under the high-speed and high-temperature gas environment in the burner bench facility. SiC inner coating was prepared by CVD method, YbDS outer coating was prepared by the sol-gel method united with air spraying. The phase composition, microstructure, oxidation and thermal cycling behavior of bi-layer YbDS/SiC EBCs covered C_f/SiC composites at high-speed and high-temperature gas environments were particularly discussed.

Experimental

2.1 Coating preparation

All the materials used for YbDS and YbDS precursor synthesis were of the analytical reagent grade (AR). The YbDS powder and YbDS precursor synthesis were synthesized by a sol-gel process, and the details of them were reported in Ref [24， 25]. The average diameter of YbDS powder is controlled below 5 μm to meet the compactness and uniformity of the coating. The round specimen size of burner rig tests specimen (25 mm diameter and 5 mm thick) is cut from a bulk 2.5 D C_f/SiC composites, which manufactured by polymer infiltration pyrolysis (PIP) method [26]. All specimens should be cleaned and dried at 353 K for 5 h after hand-polished using 600 and 1000 grit diamond grinding discs.

The SiC inner layer coating was deposited on the external of PIP C_f/SiC composites by CVD method, the deposition temperature and time are 1473 K and 30 h, respectively. YbDS outer layer coating was prepared on the external of SiC coating by sol-gel method united with air spraying, the detailed preparation process of YbDS precursor suspension and spraying parameters during the spraying process were referenced our previous work [24, 27-29].

2.2 Burner rig tests

The high-speed gas scouring experiment of the circular specimen on the burner bench facility made by our laboratory is shown in **Fig. 1**. Standard aviation-grade kerosene (No. 3 jet fuel) was used as the fuel of burner bench facility experiment. By controlling the ratio of aviation-grade kerosene and high purity oxygen in the facility, the complete combustion of aviation-grade kerosene was realized to form the main products CO_2 and H_2O. Firstly, fix the circular specimen on the ceramic holder, and then quickly heated the specimen in the high-speed and high-temperature gas environment after the formation of a stable high-speed and high-temperature gas. The temperature at the center of the specimen surface was measured by an infrared temperature measuring instrument (MR1SBSF, Raytek, USA). Subsequently, the ratio of

high purity oxygen and aviation-grade kerosene was adjusted rapidly to stabilize the surface temperature of the specimen at 1773±20 K, and then held at this temperature for 15 min. The specimens were directly removed from the high-speed gas flame and cooled to room temperature with compressed air in 1 min, and then weighed by the electronic balance after it cooled to room temperature. Eventually, the specimens were placed into the high-speed and high-temperature gas flame again for the next burner rig tests. The weight change data in a unit surface area were collected after every two cycles, and the weight change of unit surface area was calculated by the formula (1):

where *WL* is the weight change of the covered specimens, g·cm^{-2}. m_0 is the starting weight of the covered specimens, g. m_1 is the weight of the covered specimens after a certain cycles, g *s* is the external area of covered specimen, cm^2.

$$WL = (m_0 - m_1) / s \times 100\% \quad (1)$$

2.3 Coating characterization

The phases of the coatings before and after burner rig tests were identified by X-ray diffraction (XRD, Rigaku D/max 2550, Japan) with a Cu radiation operating at 40 kV and 200mA. The morphology and elemental distribution of the coatings before and after burner rig tests were analyseed by a scanning electron microscope (SEM, Nova NanoSEM230, Japan) equipped with energy dispersive spectroscopy (EDS) at 20.0 kV. The 3D erosive surface of the coating after burner rig tests were analyzed by super-high magnification lens zoom 3D microscopy (VHX-5000, Japan).

Results And Discussion

3.1 Microstructure and phase of the bi-layer EBCs

Surface XRD patterns and SEM images of bi-layer YbDS/SiC coating are shown in **Fig. 2**. There are only the diffraction peaks of SiC and YbDS phases on the external of SiC inner coating and YbDS outer coating, respectively. There are no diffraction peaks of the SiC phases detected on the external of YbDS outer coating, which shows that the thickness of YbDS outer coatings is uniform without obvious defects. Meanwhile, no macroscopic cracks are detected on the external of SiC inner coating and YbDS outer coating in circular specimens, respectively, which shows that a dense and uniform coating can be prepared on the external of special shaped specimens by the CVD method and the sol-gel united with air spray method. SEM images show that the SiC coating prepared by CVD method is very compact and with the typical “pebble-like” morphology. After high-temperature sintering, no visible cracks are detected on the external of YbDS outer coating owing to the good match in CTE between SiC and YbDS ceramics. However, there are some micro-holes in YbDS outer coating due to the volatilization of solvents during the process of coating preparation.

Fig. 3 shows the cross-section SEM image of bi-layer YbDS/SiC coating covered C_f/SiC composites. As can be seen from Fig. 3(a), the bi-layer YbDS/SiC coating is uniformly, and compactly deposited on the external of C_f/SiC matrix, which can effectively protect the contact between the matrix and the external oxidation environment. Meanwhile, the surface of YbDS outer coating prepared by sol-gel united with air spray method is very smooth and the thickness distribution is uniform. Fig. 3(b) shows that the average thickness of bi-layer YbDS/SiC coating is about 70 μm, and the average thickness of SiC inner coating, YbDS outer coating are about 30 μm, and 40 μm, respectively. Moreover, the interface between SiC inner coating and C_f/SiC substrate, YbDS outer coating and SiC inner coating are closely bonded, and no penetrating cracks are detected in YbDS/SiC coating.

Fig. 4 shows the map elements distribution (Yb, Si, O) in the cross-profile of bi-layer YbDS/SiC coating covered C_f/SiC composites. As can be seen from Fig. 4(a), the structure distribution of each layer in the bi-layer YbDS/SiC coating is very obvious. Figs. 4(b) to (d)) shows the obvious Yb, Si, and O elements in YbDS outer coating. Fig. 4(c) shows the obvious Si element in SiC inner coating and C_f/SiC composites. All the element distribution diagrams (Figs. 4(a) to (d)) show that the chemical stability between each coating and C_f/SiC composites is good, and no element diffusion of Yb, Si, O is detected.

3.2 Gas erosion resistance of the bi-layer EBCs

Fig. 5 shows the surface macrophotograph of bi-layer YbDS/SiC coating covered C_f/SiC composites during thermal cycle process between 1773 K and room temperature in the burner rig tests. Fig. 5(a) shows that no visible cracks are detected on the external of bi-layer YbDS/SiC coating covered C_f/SiC composites in the initial state. Meanwhile, there are still no visible cracks detected on the external of bi-layer YbDS/SiC coating covered C_f/SiC composites after 12 thermal cycles (180 min) at 1773 K (Fig. 5(b)). This is mainly attributed to the close CTE of the SiC inner coating and the YbDS outer coating. However, after 24 thermal cycles (360 min), the visible cracks began to appear on the local and edge of the bi-layer coating (Fig. 5(c)). With the increase of thermal cycles between 1773 K and room temperature in the burner rig, the number and width of visible cracks on the external of the coating covered C_f/SiC matrix are gradually increased (Figs. 5(d) to (f)). After 36 thermal cycles (540 min) at 1773 K, there are a lot of visible cracks not only on the surface but also on the arc edge of the bi-layer YbDS/SiC coating covered specimen (Fig. 5(f)). At the same time, no obvious coating shedding phenomenon was found due to the better bonding strength between YbDS outer coating and SiC inner coating.

Fig. 6 shows the weight change curves of bi-layer YbDS/SiC coating covered C_f/SiC composites with the thermal cycle process between 1773 K and room temperature in the burner rig. See in Fig. 6, the oxidation behavior of the YbDS/SiC coating covered C_f/SiC specimen in high-speed and high-temperature gas environment can be divided into two stages denoted as A and B. A stage is a stable oxidation stage (0-300 min), the weight change of the YbDS/SiC coating covered specimens is steadily and slowly increased with the oxidation time. After 20 thermal cycles (300 min) at 1773 K, the weight change of the covered specimen is only 5.93×10^{-3} g·cm^{-2}, which shows a good oxidation resistance of the bi-layer

YbDS/SiC coating for C_f/SiC specimen in A stage. However, the weight change of the covered specimen is rapidly increased in B stage (300-540 min). As can be seen from the macrophotograph of Fig. 5, the reason for the rapid increase of weight change is the formation of visible cracks on the external of YbDS/SiC coating. After 36 thermal cycles (540min) at 1773 K, the weight change of the covered specimen is 37.67×10^{-3} g·cm^{-2}, which indicates that the weight change of the covered specimen has entered the rapid oxidation stage.

Fig. 7 shows the **s**urface SEM images of bi-layer YbDS/SiC coating covered C_f/SiC composites with different thermal cycles between 1773 K and room temperature in the burner rig. After 24 thermal cycles (360 min) at 1773 K, a large number of micro-cracks are found on the external of YbDS/SiC coating except for a few visible cracks, this micro-cracks provide a channel for oxygen diffusion to the C_f/SiC matrix, and resulting in partial oxidation of the carbon fibers and matrix in C_f/SiC composites. The above phenomenon is the reason for the stable oxidation of covered specimen in A stage (Fig. 6). However, as the number of thermal cycles increases to 36 (540 min), there are a lot of cracks with a wider size on the external of YbDS/SiC coating (Fig. 7(b)). Meanwhile, a large number of cracks can be seen on the external of YbDS/SiC coating at the edge of the circular specimen. The oxygen content diffused into the C_f/SiC substrate by YbDS/SiC coating is greatly increased due to the increase of the number and width of cracks, and resulting in the rapid increase of the weight change of the specimen in B stage (Fig. 6). The EDS analysis on the external of YbDS coating in Fig. 7(b) shows that the atomic percentage ratio of each element in YbDS coating is approximately in accord with that of 2:2:7, respectively (Fig. 7(d)). This indicates that the YbDS coating has very good chemical stability under a high-speed and high-temperature gas environment.

Fig. 8 shows the cross-section SEM images of bi-layer YbDS/SiC coating covered C_f/SiC composites after 36 thermal cycles (540 min) between 1773 K and room temperature in the burner rig. Compare with the bi-layer YbDS/SiC coating covered C_f/SiC specimen before thermal cycles (Fig. 3(a)), the surface of YbDS outer coating becomes rough and the thickness distribution of YbDS outer coating becomes uneven after 36 thermal cycles in high-speed and high-temperature gas environment (Fig. 8(a)), which caused by the continuous erosion of YbDS outer coating by high-speed gas. Fig. 8(b) shows that the crack on the external of YbDS/SiC coating can be divided into penetrating cracks and non-penetrating cracks. The penetrating cracks in bi-layer YbDS/SiC coating are caused by the difference of CTE between integral YbDS/SiC coating and C_f/SiC composites. Meanwhile, the non-penetrating cracks are caused by the difference of CTE between YbDS outer coating (~4.1×10^{-6}/K) and SiC inner coating (4.3-5.4 × 10^{-6}/K). Fig. 8c shows the penetrating crack in YbDS/SiC coating, the oxygen diffuses into C_f/SiC matrix through penetrating cracks, and resulting in rapid oxidation of carbon fibers and matrix near the penetrating cracks. As can be seen from Figs. 8(b) and (c), there are a large number of pores left by the oxidation of carbon fibers. Fig. 8(d) shows the interface between YbDS outer coating and SiC inner coating after 36 thermal cycles (540 min), the interface is still tightly bonded and has a very obvious SiO_2 film due to the oxidation of SiC coating surface in 1773 K.

In order to find out the reason why the surface of bi-layer YbDS/SiC coating becomes rough after thermal cycles in high-speed and high-temperature gas environment. **Fig. 9** shows the surface 3D morphology of bi-layer YbDS/SiC coating after 36 thermal cycles (540 min) to better observe the three-dimensional structure on the external of the coating. There is a very obvious annular corrosion pit area on the external of YbDS outer coating, and two cracks are intersected in the center of the corrosion pit area. According to the distribution curve of the depth in the coating section, an obvious arc-shaped corrosion pit curve is gradually formed after high-speed and high-temperature gas corrosion. The above results show that in high temperature and high-speed gas environment, it is easy to form annular corrosion pits on the external of YbDS outer coating in the region of higher gas velocity. Meanwhile, the center of the corrosion pit is easier to be the origin area of the crack due to the greater impact force of the gas.

Conclusion

1. In the early stage of thermal cycle, bi-layer YbDS/SiC coating shows better oxidation resistance for C_f/SiC specimens in gas scour environment owing to the matching of CTE between SiC inner and YbDS outer coatings, which can prevent the oxidation of C_f/SiC specimens at 1773 K for 20 thermal cycles (300 min) with a weight change of 5.93×10^{-3} g·cm^{-2}.
2. After 20 thermal cycles (≥300 min), the weight change of bi-layer YbDS/SiC covered specimen is rapidly increased due to the formation of penetrating cracks in YbDS/SiC coating. The penetrating cracks provide a channel for oxygen diffusion to the C_f/SiC substrate, which leads to the rapid oxidation of the substrate. After 36 thermal cycles (540 min), the weight change of the covered specimen reaches67×10^{-3} g·cm^{-2}.
3. After 36 thermal cycles (540 min) of corrosion in high-speed and high-temperature gas, there are some obvious annular corrosion pit area on the external of YbDS outer coating, and the center of the corrosion pit is easier to be the origin area of the cracks due to the greater impact force of the gas.

Declarations

Acknowledgments

This work was supported by the the Natural Science Foundation of Hunan Province of China (Grant No. 2019JJ50768) and Graduate degree thesis Innovation Foundation of Central South University (Grant No. 2019zzts855)..

References

1. Li, P. Xiao, H. Luo, et al. Fatigue behavior and residual strength evolution of 2.5D C/C-SiC composites, J. Eur. Ceram. Soc. 36(16) (2016) 3977-3985.
2. J. Tang, C.L. Hu, S.Y. Pang, et al. Interfacial modification and cyclic ablation behaviors of a SiC/ZrB_2-SiC/SiC triple-layer coating for C/SiC composites at above 2000°C, Corros. Sci. 169 (2020) 108604.

3. Z. Fan, W.Z. Huang, H.T. Liu, et al. Bond stability and oxidation resistance of BSAS-based coating on C/SiC composites, Surf. Coat. Tech. 309 (2017) 35-46.
4. Wang, L. Cheng, L. Xiang, et al. Effect of SiC coating and heat treatment on the thermal radiation properties of C/SiC composites, J. Eur. Ceram. Soc. 34(7) (2014) 1667-1672.
5. Li, P. Xiao, Z. Li, et al. Strength evolution of cyclic loaded LSI-based C/C-SiC composites, Ceram. Int. 42(13) (2016) 14505-14510.
6. Yang, C. Feng. Effects of ZrC coating on mechanical properties of PIP-C/SiC composites, J. Alloy. Compo. 632 (2015) 263-268.
7. Rizvanbasha, A. Udayakumar, M. Stalin, et al. Vapour phase synthesis and characterisation of Cf/SiC composites with selfhealing Si-B-C monolayer coating, Ceram. Int. 46(15) (2020) 23785-23796.
8. T. Wang, L.Y. Cao, J.F. Huang, et al. A mullite/SiC oxidation protective coating for carbon/carbon composites, J. Eur. Ceram. Soc. 33(1) (2013) 191-198.
9. Li, P. Xiao, Z. Li, et al. Oxidation behavior of C/C composites with SiC/$ZrSiO_4$-SiO_2, coating, Trans. Nonferrous Met. Soc. China. 27(2) (2017) 397-405.
10. Liu, L.T. Zhang, Q.M. Liu, et al. Structure design and fabrication of environmental barrier coatings for crack resistance, J. Eur. Ceram. Soc. 34(8) (2014) 2005-2012.
11. G. Zhang, W. J. Fan, B.L. Zou, et al. Microstructure and oxidation resistant behavior of $Er_2Si_2O_7$, and $Er_2Si_2O_7$/$LaMgAl_{11}O_{19}$, coatings deposited on C_f/SiC composites by APS at 1723K, J. Alloy. Compd. 709 (2017) 24-30.
12. T. Wang, L.Y. Cao, J.F. Huang, et al. Microstructure and oxidation resistance of C-$AlPO_4$ -mullite coating prepared by hydrothermal electrophoretic deposition for SiC-C/C composites, Ceram. Int. 39(2) (2013) 1037-1044.
13. W. Song, U. Y. Paik, X.Y. Guo, et al. Microstructure design for blended feedstock and its thermal durability in lanthanum zirconate based thermal barrier coatings, Surf. Coat. Tech. 308 (2016) 40-49.
14. X. Wang, W. Li, S. Wang, et al. Deposition of SiC/La2Zr2O7 multi-component coating on C/SiC substrate by combining sol-gel process and slurry, Surf. Coat. Tech. 302 (2016) 383-388.
15. C. Su, C.H. Yi. Effects of CMAS penetration on the delamination cracks in EB-PVD thermal barrier coatings with curved interface, Ceram. Int. 43(12) (2013) 8893-8897.
16. T. Martin, C. Bennett, T. Hussain. A review on environmental barrier coatings: History, current state of the art and future developments, J. Eur. Ceram. Soc. 41(3) (2021) 1747-1768.
17. C. Ren, E. Feng, Y.L. Zhang, et al. Microstructure and anti-ablation performance of HfC-TaC and HfC-ZrC coatings synthesized by CVD on C/C composites, Ceram. Int. 46(8) (2020) 10147-10158.
18. Bernard, A. Quet, L. Bianchi, et al. Thermal insulation properties of YSZ coatings: Suspension Plasma Spraying (SPS) versus Electron Beam Physical Vapor Deposition (EB-PVD) and Atmospheric Plasma Spraying (APS), Surf. Coat. Tech. 318 (2016) 122-128.
19. L. Wen, P. Xiao, Z. Li, et al. Microstructure and oxidation behavior of sol-gel mullite coating on SiC-coated carbon/carbon composites, J. Eur. Ceram. Soc. 35(14) (2015) 3789-3796.

20. J. Chen, P. Xiao, Z. Li, et al. Oxidation properties of tri-layer ytterbium-disilicate/mullite/silicon-carbide environment barrier coatings for C_f/SiC composites, Surf. Coat. Tech. 402 (2020) 126329.
21. L. Stokes, B.J. Harder, V.L. Wiesneret, et al. High-Temperature thermochemical interactions of molten silicates with $Yb_2Si_2O_7$ and $Y_2Si_2O_7$ environmental barrier coating materials, J. Eur. Ceram. Soc. 39(15) (2019) 5059-5067.
22. Q. Wang, J.L. Liu. First-principles investigation on the corrosion resistance of rare earth disilicates in water vapor, J. Eur. Ceram. Soc. 29(11) (2009) 2163-2167.
23. Maier, K.G. Nickel, G. Rixecke. High temperature water vapour corrosion of rare earth disilicates $(Y,Yb,Lu)_2Si_2O_7$ in the presence of $Al(OH)_3$ impurities, J. Eur. Ceram. Soc. 27(7) (2007) 2705-2713.
24. J. Chen, L. Pan, P. Xiao, et al. Microstructure and anti-oxidation properties of $Yb_2Si_2O_7$/SiC bilayer coating for C/SiC composites, Ceram. Int. 45(1) (2019) 854-860.
25. Zhao, F. Wang, Y.J. Sun, et al.. Synthesis and characterization of β-$Yb_2Si_2O_7$ powders, Ceram. Int. 39(5) (2013) 5805-5811.
26. Wen, S. Zhou, Y. Lu, et al. Oxidation behavior and high-temperature flexural property of CVD-SiC-coated PIP-C/SiC composites, Ceram. Int. 44(14) (2018) 16583-16588.
27. J. Chen, P. Xiao, Z. Li, et al. Microstructure and oxidation behavior of a novel bilayer (c-$AlPO_4$–SiC_w–mullite)/SiC coating for carbon fiber reinforced CMCs, J. Eur. Ceram. Soc. 39(14) (2019) 3988-3999.
28. J. Chen, P. Xiao, Z. Li, et al. Effect of residual silicon on the oxidation resistance of bi-layer $Yb_2Si_2O_7$/SiC coated C/SiC composites at high temperature, Corros. Sci. 170 (2020) 108676.
29. J. Chen, P. Xiao, Z. Li, et al. Bonding strength and thermal shock resistance of a novel bilayer (c-$AlPO_4$–SiC_w–mullite)/SiC coated carbon fiber reinforced CMCs, J. Am. Ceram. Soc. 103 (2019) 82-93.

Figures

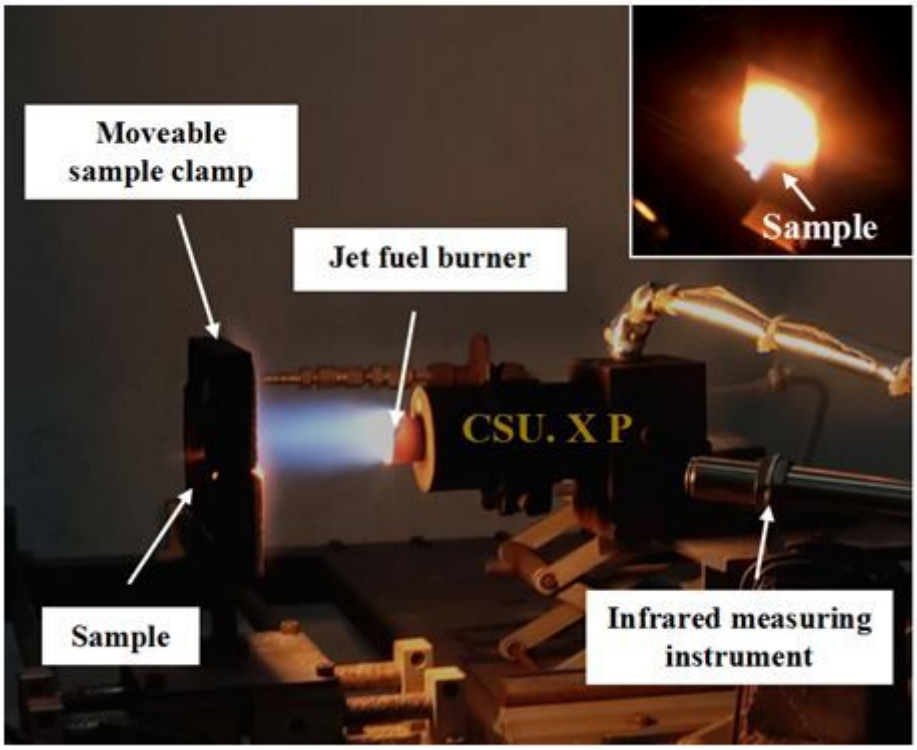

Figure 1

Photograph of a circular specimen under the burner rig test in burner bench facility.

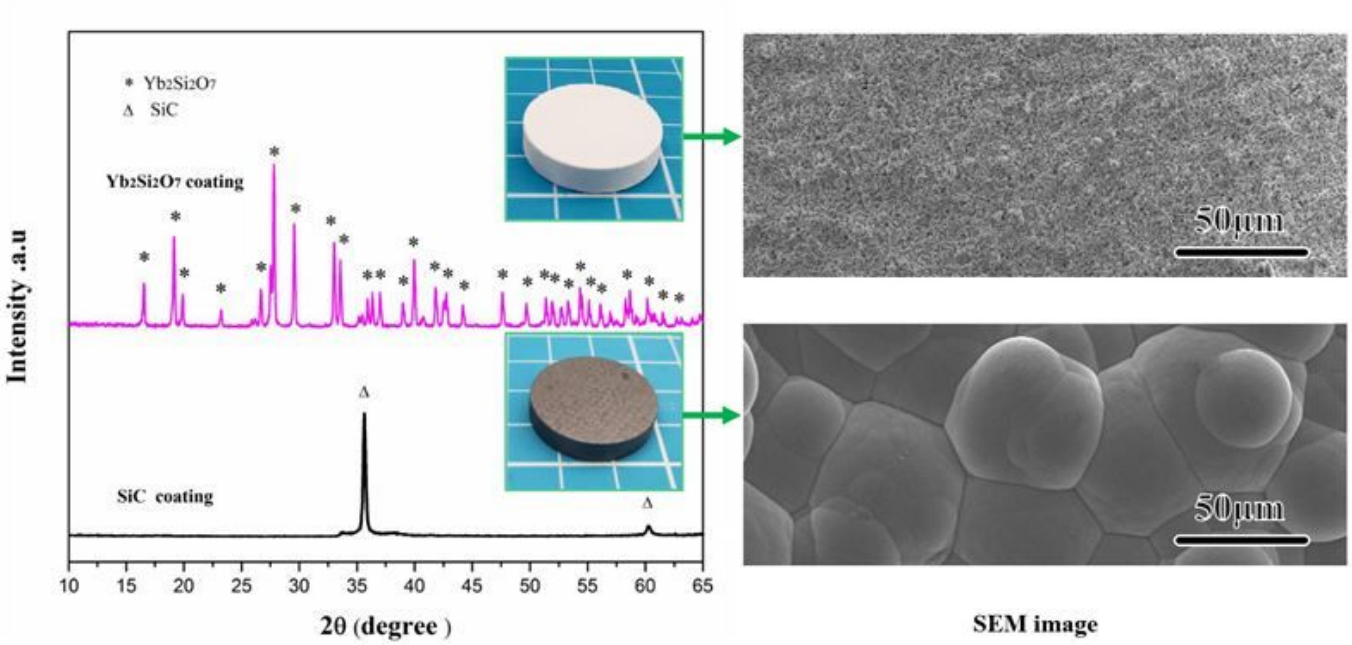

Figure 2

Surface XRD patterns and SEM image of different coating in bi-layer YbDS/SiC coating covered Cf/SiC composites.

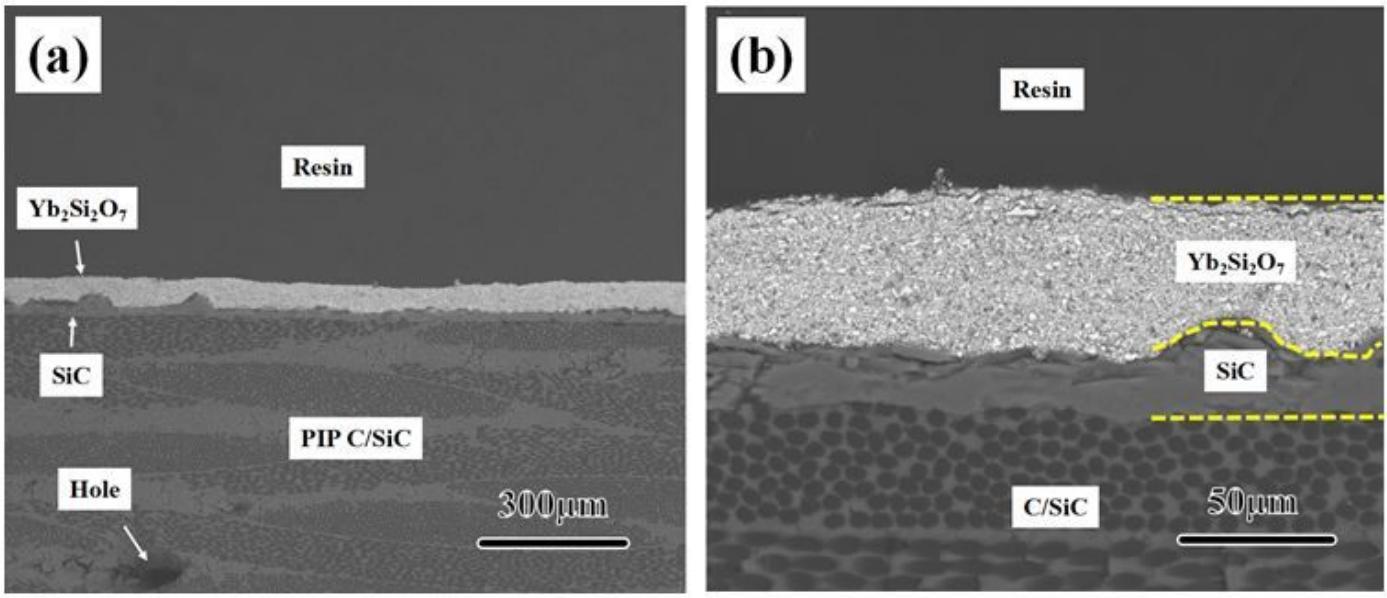

Figure 3

Cross-section SEM image of bi-layer YbDS/SiC coating covered Cf/SiC composites.

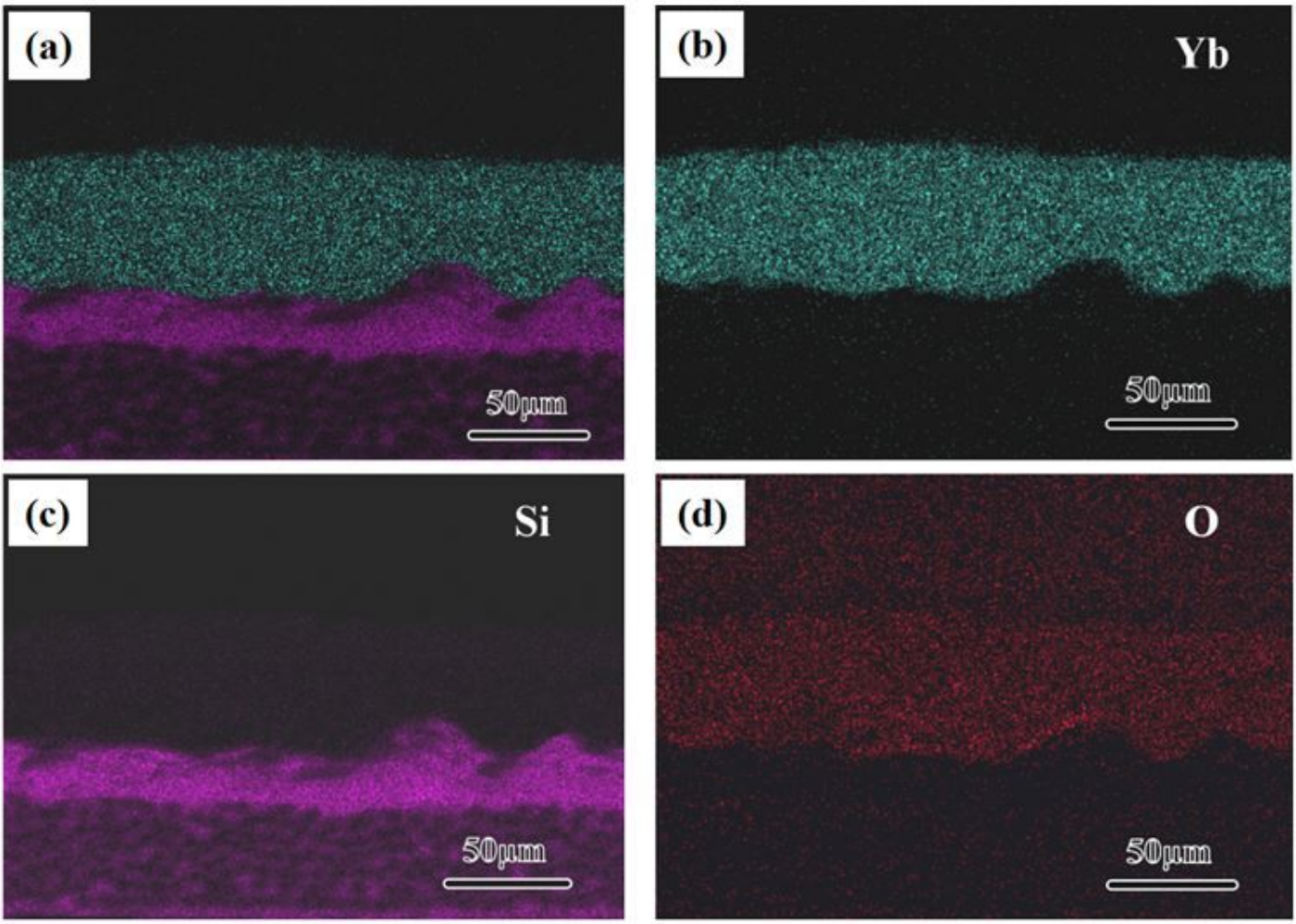

Figure 4

Cross-section EDS element map scan analysis of bi-layer YbDS/SiC coating covered Cf/SiC composites.

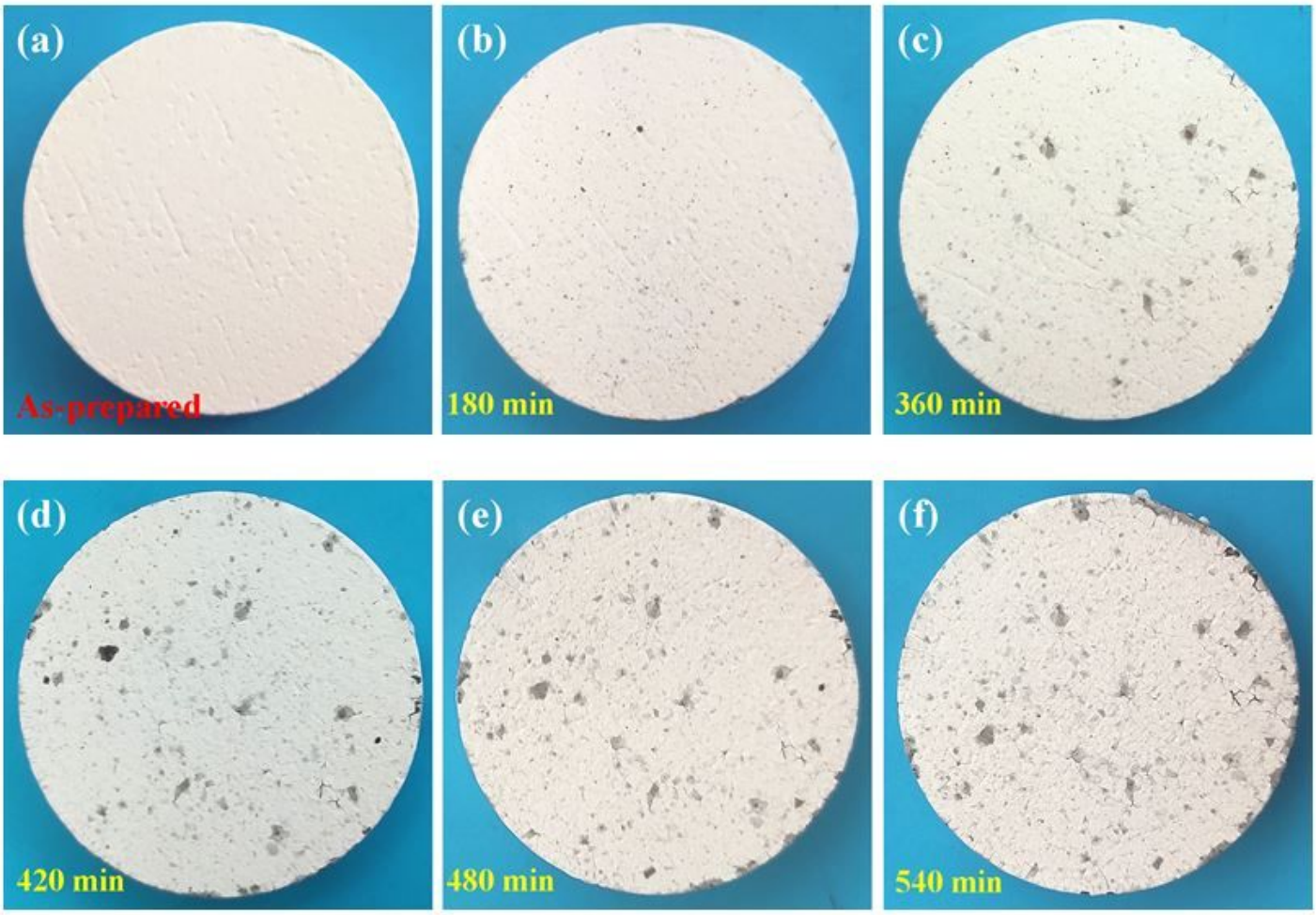

Figure 5

Surface macrophotograph of bi-layer YbDS/SiC coating covered Cf/SiC composites with the oxidation time/thermal cycle (15min/cycle).

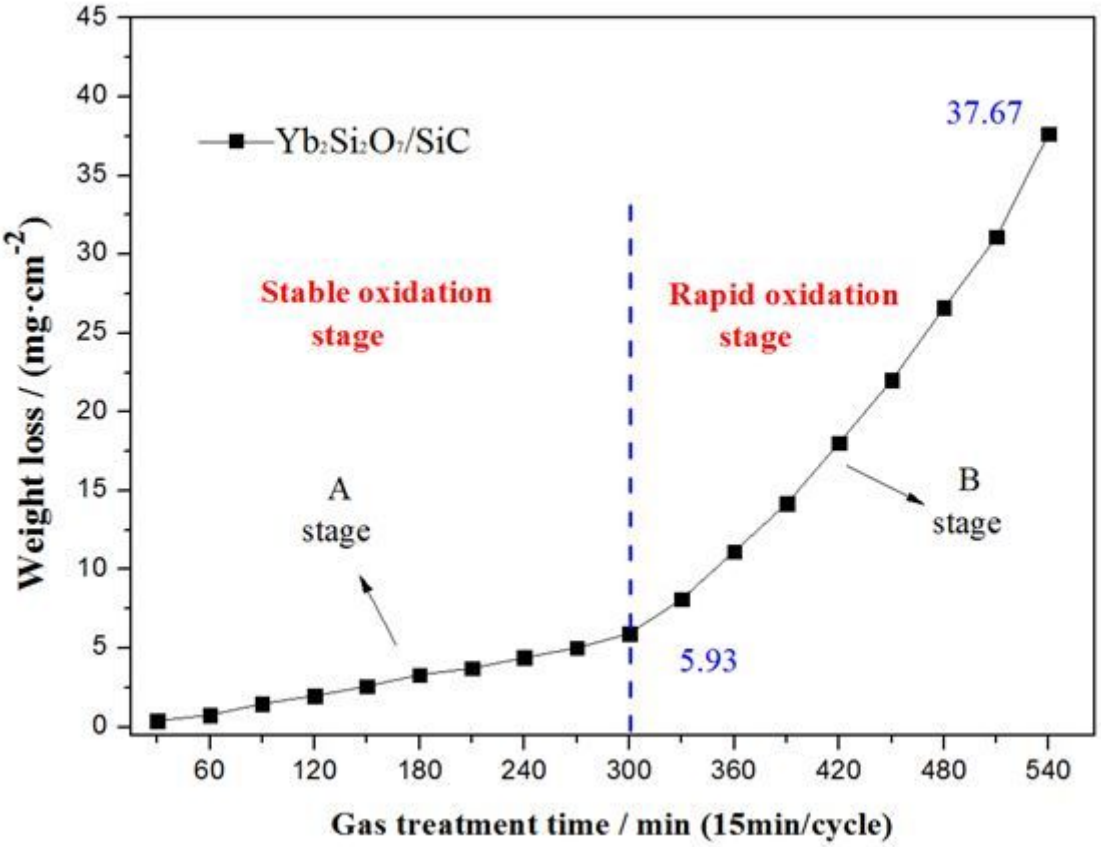

Figure 6

Weight change curves of bi-layer YbDS/SiC coating covered Cf/SiC composites with the oxidation time/thermal cycle (15min/cycle).

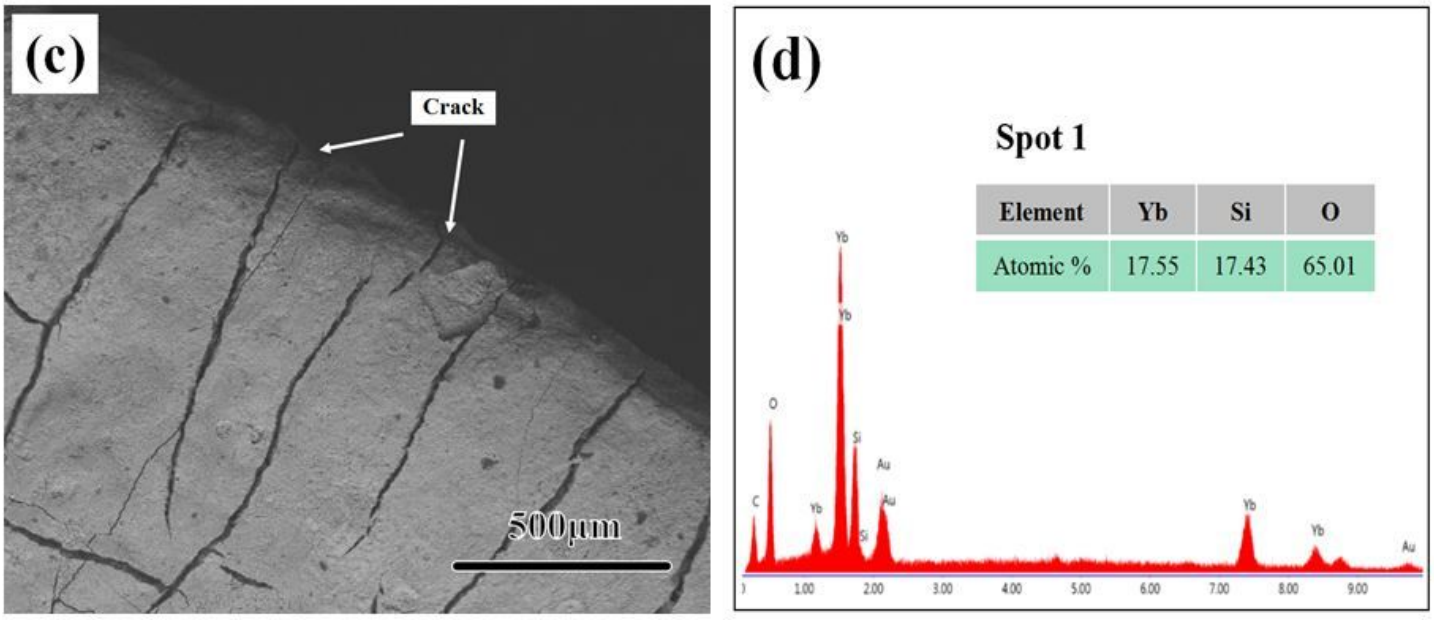

Figure 7

Surface SEM images of bi-layer YbDS/SiC coating covered Cf/SiC composites with different thermal cycles (15min/cycle) at 1773 K, (a) 360 min; (b-d) 540 min.

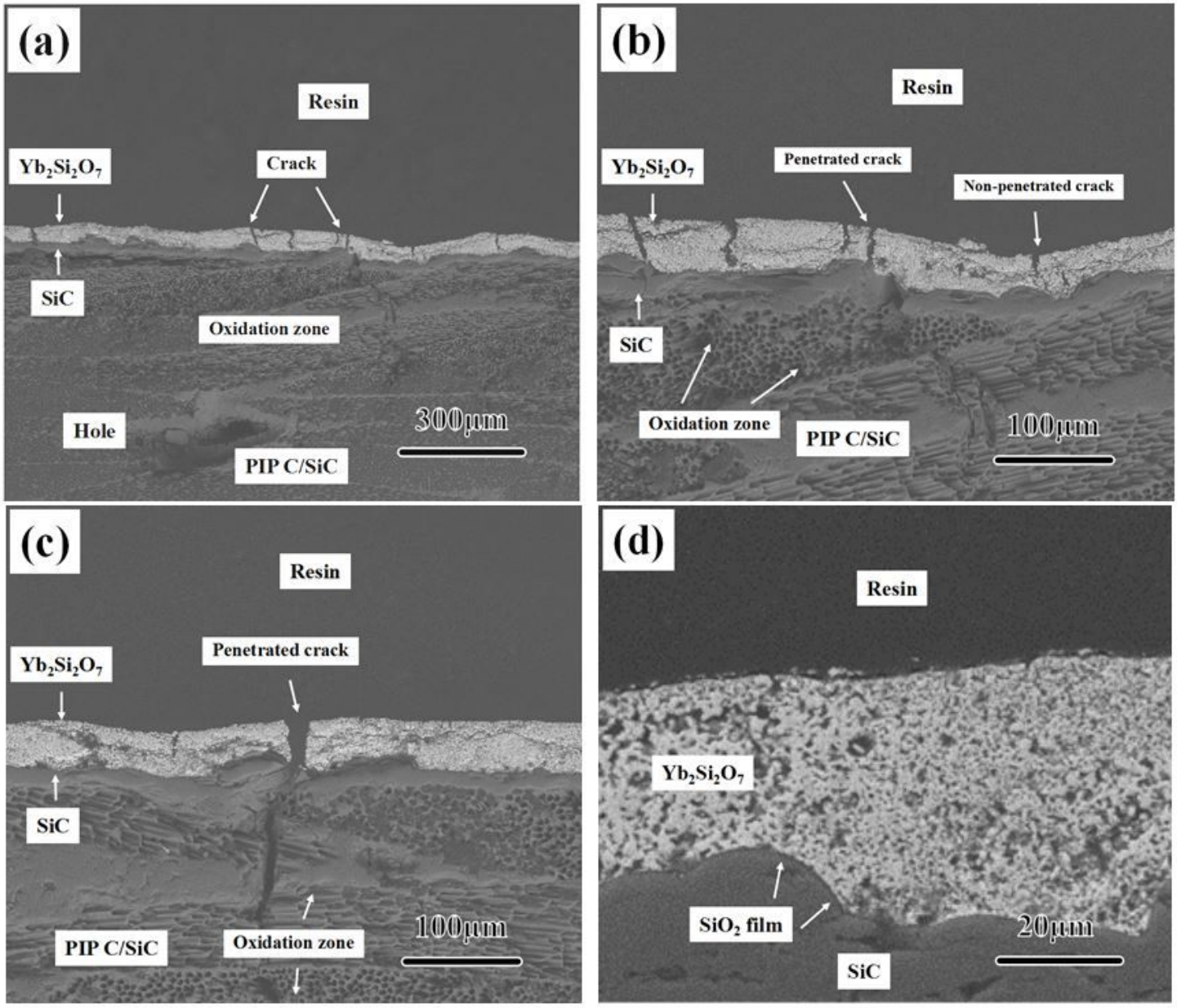

Figure 8

Cross-section SEM images of bi-layer YbDS/SiC coating covered Cf/SiC composites after 36 thermal cycles (15min/cycle) at 1773 K..

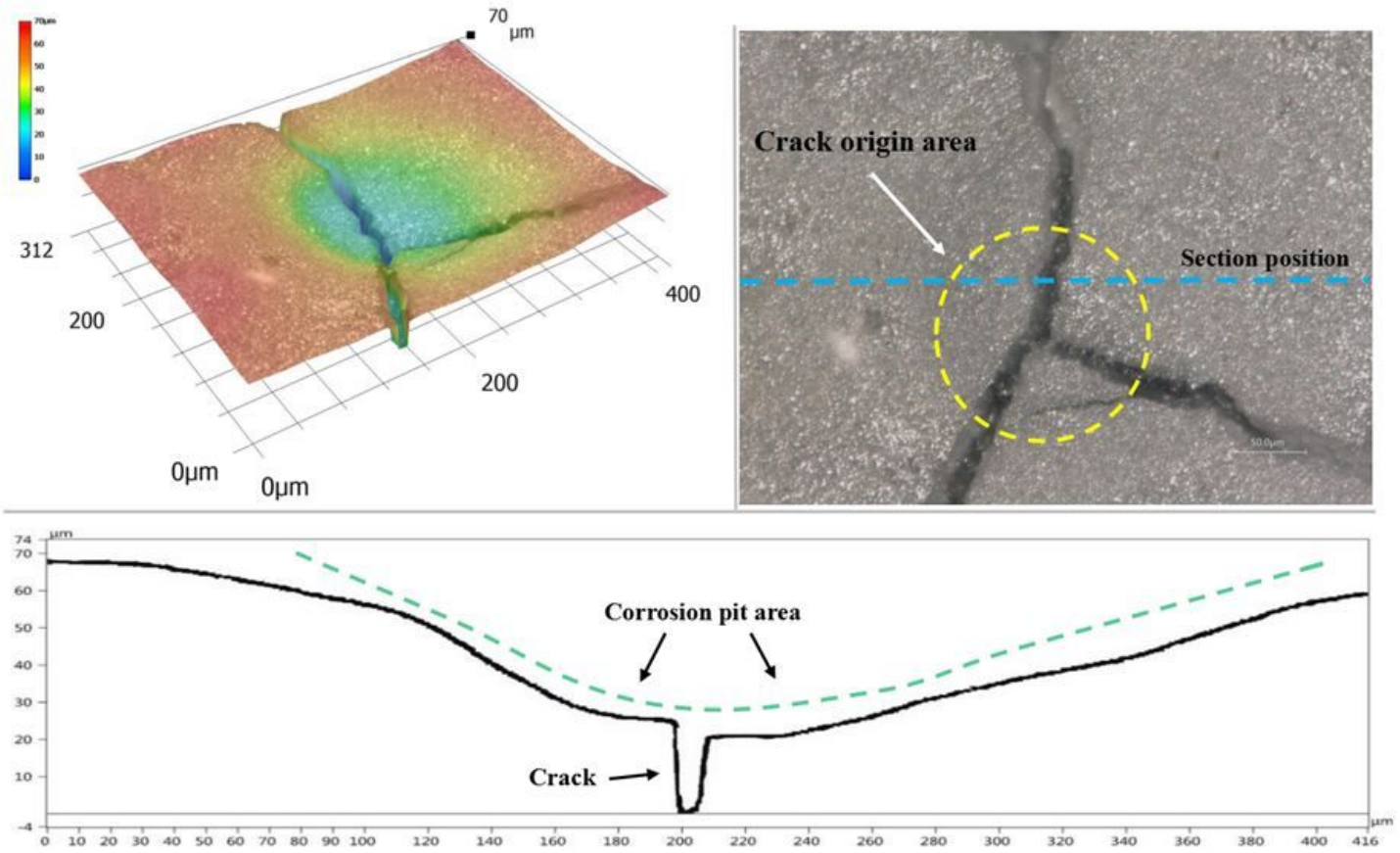

Figure 9

Surface 3D morphology of bi-layer YbDS/SiC coating covered Cf/SiC composites after 36 thermal cycles (15min/cycle) at 1773 K.